$C(sp^2)-C(sp^3)$ Rotational Barriers in Simple Amides: $H_2N-C(=O)-R$ (R = Methyl, Ethyl, i-Propyl, *tert*-Butyl)

Giovanni Sandrone, David A. Dixon, and Benjamin P. Hay*

Theory, Modeling, and Simulation Group, Environmental Molecular Science Laboratory, Pacific Northwest National Laboratory, Richland, Washington 99352

Received: June 16, 1998; In Final Form: October 9, 1998

Potential energy surfaces for rotation about the $C(sp^2)-C(sp^3)$ bond are reported for acetamide, propanamide, 2-methylpropanamide, and 2,2-dimethylpropanamide at different levels of ab initio electronic structure theory with correlation effects included. In all cases, fully optimized geometries of rotational minima are consistent with gas phase electron diffraction data and crystal structure data. The experimental barrier height for methyl rotation in acetamide is reproduced to within 0.1 kcal/mol. This study yields a set of improved criteria for the construction of rotational potentials for the C_a-C bond which are used to obtain improved MM3 torsional parameters. In addition, we find that the use of higher levels of theory leads to significantly different results than those obtained in prior Hartree−Fock studies on acetamide and 2-methylpropanamide.

Introduction

Amides are a class of molecules important to several chemical disciplines. Not only are they a major functional group in organic chemistry[1] but they form key linkages in natural macromolecules such as proteins and polypeptides and synthetic macromolecules such as nylons and Kevlar. Amides also contain oxygen and nitrogen heteroatoms that can coordinate with metal ions.[2,3] Ligands containing amide donor groups are potentially advantageous in a variety of applications, including their use as complexing agents for the selective extraction of actinides[4] and their use as magnetic resonance imaging (MRI) agents.[5]

Our current research involves the development of structure−function relationships to allow the design of multidentate amide ligands with enhanced metal ion affinity and selectivity. In the course of this work we have completed an extended MM3 force field for amide complexes with the alkali and alkaline earth cations, transition metals, lanthanides, and actinides.[6] The parametrization and validation of the MM3 model involved the examination of a large number of crystal structures. A review of the structures of metal complexes with monodentate N-alkylated amides established that metal ions prefer to lie in the plane of the amide group and cis with respect to the C_a substituent as shown in structure **1**.[3] This orientation places the C_a substituent in close contact with other ligands in the complex. It is therefore important that the amide force field correctly models the rotation about the C_a-C bonds (see **1**), with respect to the location of the minima as well as the barrier heights, in order to reproduce the structures of the metal−amide complexes. In a number of cases, however, the default MM3 amide parameters failed to yield observed ligand conformations. Exploring the cause of these failures provided the impetus for the current study.

1

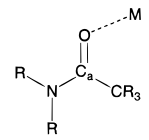

The majority of prior studies on bond rotations in amides have been motivated by the development of force fields for modeling the structure and dynamics of peptides and proteins.[7] The peptide linkage is shown in structure **2**. Because the $H(C)N-C_a=O$ components of the peptide backbone exhibit a strong tendency toward planarity, secondary protein structure is determined by the dihedral angles about C−N and C_a-C bonds. Theoretical calculations to determine the relative energies for stable conformations of dipeptides and polypeptides have been used in the parametrization and testing of protein force fields.[8] With respect to C_a-C bond rotation in amides, we note that the protein studies focus on the special case in which the $C(sp^3)$ carbon is connected to an amide nitrogen and amide nitrogens are mono-alkylated.

2

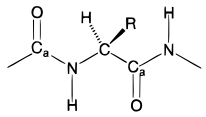

Several force fields have been specifically parametrized to reproduce specific experimental properties of the simple amides shown below (structures **3**−**8**).[9−12] An MM2 model reproduces bond lengths and bond angles, moments of inertia, dipole moments, the rotational barrier about the C_a-N bond, and the energy difference for the cis and trans N-alkylamides.[10] The MM3 model also reproduces these experimental properties as well as vibrational frequencies, heats of formation, and bond length changes on moving from gas phase to condensed phase.[12] A QMFF amide force field recently has been reported that is based solely on fitting to HF/6-31G* calculations of the aforementioned properties.[13] These studies all report the torsional parameters that are required to calculate the rotation about the C_a-C bond in any aliphatic amide. However, in no case are calculated C_a-C rotamers and rotational barriers compared with experimental data to validate the accuracy of these parameters.

10.1021/jp982649k CCC: $18.00
Published on Web 02/03/1999

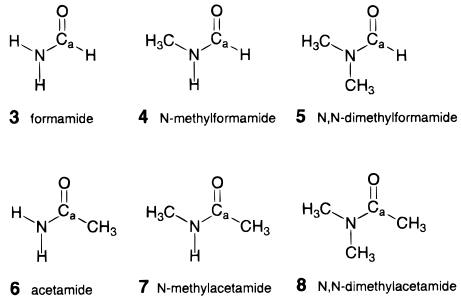

Hagler et al. noted in 1976 that experimental information concerning the C_a-C rotation in simple amides was scarce.[14] This situation has not significantly altered over the past two decades in which there have been only two reported measurements of such rotational barriers, both for methyl rotation.[15,16] The current status for the four representative types of amide C_a alkylation illustrated by **6** and **9**−**11** is that there has been only one reported measurement of the barrier to C_a-C rotation in **1**.[16] A number of theoretical investigations of methyl rotation in **6** have been reported at the Hartree−Fock level.[14,17−19] It was noted that these calculations yield an incorrect position for the rotational minima.[14] In addition, there has been one Hartree−Fock study of isopropyl rotation in **3**.[20]

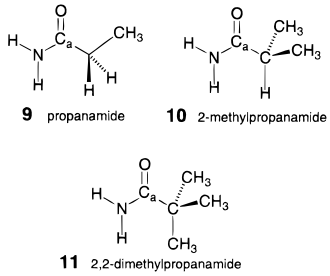

To obtain a better understanding of the C_a-C rotations in simple amides we have obtained rotational potential energy surfaces for **6** and **9**−**11** at a number of ab initio levels of theory including second-order Möller−Plesset perturbation theory (MP2) and density functional theory (DFT). We are interested in the DFT results because we are calculating the interactions of transition metal cations (singly and multiply charged) with the amide oxygen and DFT methods are the most appropriate for such calculations. The measured barrier height for **6** is reproduced to within 0.1 kcal/mol at the MP2 level. In all cases, calculated geometries of rotational minima are consistent with available gas phase electron diffraction data and crystal structure data. This study yields a set of improved criteria for the construction of rotational potentials for the C_a-C bond. We report the use of these criteria to reparametrize two MM3 torsional interactions. In addition, we find that the use of higher levels of theory leads to significantly different results than those obtained in the prior Hartree−Fock studies.

Theoretical Details

Electronic Structure Calculations. The potential energy surfaces (PESs) for torsion about the C_a-C bond in **6** and **9**−**11** were calculated by a variety of ab initio electronic structure methods. All calculations were done with the program systems Gaussian 94[21] and DGauss.[22] All calculations were done with polarized double-ζ basis sets. The PESs were obtained by constraining the torsion angle $X-C-C_a=O$ (X = H or C) and fully optimizing the remaining geometrical degrees of freedom. Intervals of 30° were used for calculating the PES of **6**, **10**, and **11**, and an interval of 15° was used for calculating the PES of **9**. The approximate locations of the minima and maxima on the PES were found by this constrained angle method. After the torsional constraints were removed, full geometry optimizations were done to obtain final geometries for the minima and maxima. Analytic second derivative calculations on the minima and maxima were then performed.

The PESs were calculated at the Hartree−Fock (HF) and second-order Möller−Plesset perturbation theory (MP2)[23,24] levels of ab initio molecular orbital (MO) theory. The HF and MP2 calculations were done with the polarized valence double-ζ basis set of Dunning and Hay.[25] The PESs were also calculated at the local density functional theory (LDFT) and nonlocal (gradient corrected) DFT (NLDFT) levels.[26] The LDFT calculations were done with Slater exchange and the Vosko, Wilk, and Nusair fit of the correlation potential of the noninteracting electron gas.[27] The NLDFT calculations were done with Becke's gradient-corrected exchange potential[28] and the Perdew-Wang gradient-corrected correlation potential.[29] The DFT calculations were done with the DZVP2 basis set and the A1 fitting set.[30] The relative energetics used to construct the PESs at the various levels are given in Table 1.

MM3 Force Field Calculations. Calculations were performed with MM3(96).[31] The development and validation of the default amide parameters provided with the program is described elsewhere.[12] This model uses several dielectric-dependent parameters to account for changes in the amide that occur on going from gas phase to condensed phase. These changes include an increased $C_a=O$ length, a decreased C_a-N length, and an increase in the barrier to rotation about the C_a-N bond. In the Results and Discussion section, gas phase parameters ($\epsilon = 1.5$) are used for comparison of results with gas phase data and MP2/dzp results and condensed phase parameters ($\epsilon = 4.0$) are used for comparison of results with crystal structure data.

Comparison of rotational potential surfaces obtained from MM3(96) versus those obtained at the MP2 level of theory revealed poor agreement as discussed in detail below. We have modified several torsional parameters to obtain a better fit. Only four types of torsional interaction terms directly affect rotation about the C_a-C bonds in **6** and **9**−**11**. These are $H-C-C_a=O$, $C-C-C_a=O$, $H-C-C_a-N$, and $C-C-C_a-N$. Parameters for two of these interactions, $H-C-C_a=O$ and $C-C-C_a=O$ were derived from work on ketones.[32] These parameters were retained and modifications were restricted to the $H-C-C_a-N$, and $C-C-C_a-N$ interaction terms.

The V_3 term for the $H-C-C_a-N$ (MM3 atom types 5−1−3−9) interaction was changed from the default value of 0.230 to −0.254 kcal/mol to obtain a fit to the rotational potential surface of **6**. Then the V_1, V_2, and V_3 terms for the $C-C-C_a-N$ (atom types 1−1−3−9) interaction were modified to obtain the best simultaneous fit to the rotational potential surfaces of **9** and **10**: (default values) 0.700, −1.100, and 0.300 kcal/mol; (new values) −0.457, 0.097, and −0.630 kcal/mol, respectively. Calculations performed with this modified parameter set are termed MM3+ to distinguish them from those performed with the default MM3 parameters. MM3+ was tested by its ability to predict the rotational potential surface of **11**.

Results and Discussion

Ethanamide (6). The MP2 calculations yield a PES for the rotation of the methyl group in **6** (Figure 1) with minima in which the methyl group is staggered with respect to the $C_a=O$ bond, i.e., with one of the $H-C-C_a=O$ dihedral angles near

TABLE 1: Relative Energies (kcal/mol) for the Torsional Potential Energy Surfaces

torsion <	LDFT	NLDFT	MP2	HF
		6[a]		
0	0.35	0.27	0.21	0.05
30	0.09	0.06	0.05	0.00
60	0.00	0.00	0.00	0.01
		9[b]		
0	0.10	0.12	0.15	0.01
15	0.06	0.04	0.07	0.00
30	0.07	0.00	0.00	0.05
45	0.23	0.04	0.03	0.18
60	0.48	0.13	0.16	0.35
75	0.80	0.30	0.37	0.53
90	1.10	0.51	0.63	0.72
105	1.27	0.76	0.85	0.94
120	1.34	0.97	0.99	1.15
135	0.95	0.96	1.08	1.33
150	0.49	0.74	1.10	1.40
165	0.11	0.52	1.11	1.41
180	0.00	0.48	1.14	1.41
		10[c]		
0	1.46	1.39	1.43	1.42
30	0.79	1.12	1.34	1.40
60	0.11	0.97	1.47	1.51
90	0.47	1.50	1.79	1.76
120	0.92	1.44	1.23	1.07
150	0.44	0.54	0.44	0.27
180	0.00	0.00	0.00	0.00
210	0.40	0.49	0.39	0.21
240	0.84	1.28	1.26	0.93
270	0.63	1.60	1.79	1.74
300	0.15	1.10	1.54	1.58
330	0.61	1.00	1.32	1.39
360	1.46	1.39	1.43	1.42
		11[d]		
0	1.28	0.88	0.37	0.18
15	0.97	0.69	0.39	0.22
30	0.46	0.35	0.28	0.19
45	0.10	0.08	0.08	0.06
60	0.00	0.00	0.00	0.00

[a] Minimum energy: E(LDFT) = −207.584 235 au; E(NLDFT) = −209.269 958 au; E(MP2) = −208.637 324 au; E(HF) = −208.030 043 au. [b] Minimum energy: E(LDFT) = −246.541 425 au; E(NLDFT) = −248.632 604 au; E(MP2) = −247.821 454 au; E(HF) = −247.073 390 au. [c] Minimum energy: E(LDFT) = −285.500 617 au; E(NLDFT) = −287.909 212 au; E(MP2) = −287.008 547 au; E(HF) = −208.030 043 au. [d] Minimum energy: E(LDFT) = −324.460 344 au; E(NLDFT) = −327.225 893 au; E(MP2) = −326.195 251 au; E(HF) = −325.155 920 au.

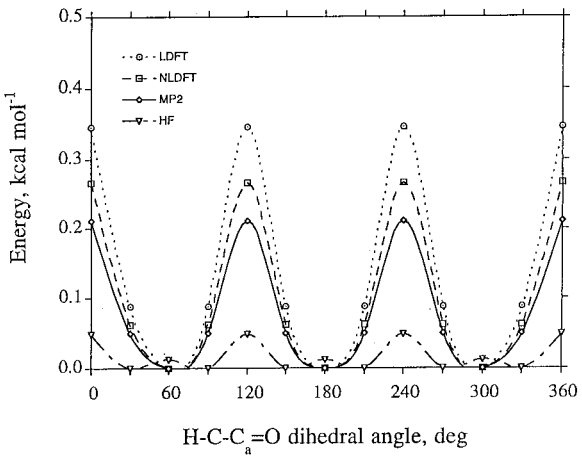

Figure 1. PES for **6** at various levels of theory.

180°. The fully optimized geometry for the minimum energy structure is shown in Figure 2 with important geometry

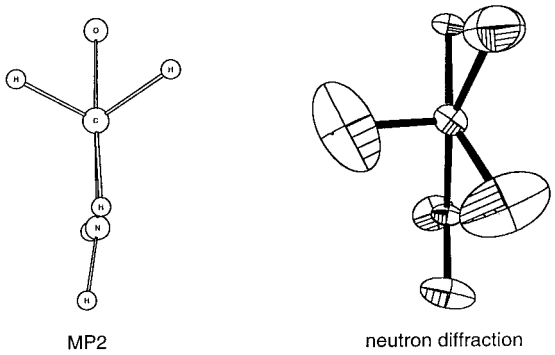

Figure 2. Comparison of the MP2 minimum energy structure and the neutron diffraction crystal structure of **6** with thermal ellipsoids shown at 50% probability.[17]

parameters in Table 2. The coordinates of the optimized structures are given as Supporting Information. In the absence of any torsional constraint the methyl group twists only 2° away from 180° to 178°. The barrier to rotation of the CH_3 group is very small, only 0.21 kcal/mol. This result is consistent with the only experimental value reported for methyl rotation in **6,** 0.07 kcal/mol determined by gas-phase microwave spectroscopy.[16]

The PES at the other theoretical levels, HF, LDFT, and NLDFT, are also shown in Figure 1. The torsional barriers are all small and increase in the order LDFT >NLDFT > MP2 > HF. The LDFT barrier is 0.35 kcal/mol and the NLDFT barrier is 0.27 kcal/mol. The HF PES shows essentially free rotation about the C−C bond with a barrier of only 0.05 kcal/mol. The very low barrier to rotation results in the energy of the conformer with $\tau = 60°$ being 0.01 kcal/mol higher than the energy of the conformer at $\tau = 30°$.

The lowest frequency harmonic modes for the minimum and transition state for **6** are given in Table 3. The HF torsional mode is 87 cm^{-1}, 0.25 kcal/mol clearly above the torsional barrier. The MP2 and NLDFT modes are much smaller at 30 and 30 cm^{-1} (0.09 kcal/mol), respectively. This suggests that at most a couple of modes are bound for the torsional surface. The zero-point differences are −0.01 kcal/mol (MP2), 0.27 kcal/mol (HF), 0.40 kcal/mol (LDFT), and 0.29 kcal/mol (NLDFT) with a positive value corresponding to a lowering of the barrier heights. The MP2 torsional surface is essentially uncorrected by zero-point motions at the harmonic level. The LDFT and NLDFT corrections are larger than the barrier height, showing that the torsional mode is strongly coupled to other modes and is likely to be quite anharmonic. The large zero-point corrections are consistent with lower barrier heights on the LDFT and NLDFT surfaces. The imaginary frequencies at the top of the barrier for the MP2 and NLDFT PESs are larger than the real torsional frequency. This further shows that the region near the top of the barrier is tighter than the region near the minimum.

Prior electronic structure calculations on **6** performed at the Hartree−Fock level all yield 3-fold rotational potentials where the minima occur with a methyl hydrogen eclipsing the C_a═O bond (minimum H−C−C_a═O dihedral angle of 0°).[14,17−19] In these calculations the calculated barriers to rotation are basis set dependent and decrease with increasing size of the basis set: 0.96 kcal/mol at STO-3G,[14] 0.41 kcal/mol with 3-21G,[17] 0.31 kcal/mol at 4-31G,[18] and 0.15 kcal/mol at 6-31G.[14] Our HF calculations with a larger polarized double ζ basis set show an even lower barrier, suggesting that even larger basis sets at the HF level should give essentially free rotation. Furthermore, these results indicate that polarization functions are required to give the correct minimum geometry.

TABLE 2: Experimental and Calculated Structural Data for 6[a]

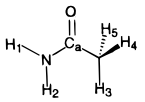

	gas phase							crystal	
		r_e				r_g	MM3+		MM3+
feature	expt ED[b]	LDFTA	NLDFT	HF	MP2	MP2[c]	($\epsilon = 1.5$)	expt ND[d]	($\epsilon \geq 4.0$)
C_a═O	1.220(3)	1.233	1.240	1.202	1.234	1.224	1.219	1.247(1)	1.235
C_a−N	1.380(4)	1.364	1.379	1.358	1.376	1.382	1.377	1.335(1)	1.336
C_a−C	1.519(6)	1.505	1.527	1.516	1.520	1.526	1.526	1.509(1)	1.526
C−H_3	1.124(10)	1.104	1.100	1.083	1.091	1.109	1.107	1.076(2)	1.107
C−H_4	1.124(10)	1.104	1.100	1.083	1.091	1.109	1.111	1.085(2)	1.111
C−H_5	1.124(10)	1.104	1.100	1.083	1.091	1.109	1.111	1.076(2)	1.111
N−H_1	1.022(11)	1.019	1.015	0.991	1.009	1.019	1.028	1.023(2)	1.028
N−H_2	1.022(11)	1.022	1.017	0.995	1.006	1.016	1.028	1.023(2)	1.028
C−C_a═O	122.9	122.2	122.2	121.7	122.6		121.3	121.1(1)	121.2
N−C_a═O	122.0(6)	121.8	121.8	122.1	122.2		122.6	122.3(1)	122.9
C−C_a−N	115.2(16)	116.0	116.0	116.2	115.2		116.0	116.5(1)	115.9
C_a−N−H_1	117.2	117.5	118.0	118.1	117.6		117.8	120.5(1)	118.4
C_a−N−H_2	120.0	122.2	122.4	122.5	121.9		120.6	120.2(1)	120.2
C_a−C−H_3	109.8(20)	108.3	108.5	108.3	113.2		112.5	112.1(1)	112.8
C_a−C−H_4	109.8(20)	108.3	108.5	108.3	108.4		110.4	110.7(2)	110.3
C_a−C−H_5	109.8(20)	114.2	114.0	113.5	108.4		110.4	108.6(2)	110.3
H_1−N−H_2	121.5	120.2	119.5	119.4	118.9		121.6	118.9(1)	121.4

[a] Bond lengths in Å, bond angles in deg. [b] Gas-phase electron diffraction. Values without uncertainties are assumed.[35] [c] MP2 r_g values were estimated from computed r_e values based on past performance.[36] [d] Neutron diffraction crystal structure (Rfac = 0.017) of **6** at 23 K.[17]

TABLE 3: Summary of Smallest Frequency, Energy Differences, and Torsion Angles for the Various Optimized Minima and Maxima

	ν_1 (cm^{-1})	iν (cm^{-1})	ZPE (kcal/mol)	ΔE (kcal/mol)	τ_{min} (deg)	τ_{max} (deg)
			6			
HF	87	57i	0.27	0.03	60.6	0.0
MP2	30	82i	−0.01	0.21	61.7	0.0
NLDFAT	33	137i	0.29	0.25	60.6	0.0
			9			
HF	190	8	−0.36	1.42	15.4	180.0
MP2	36	26i	0.13	1.14	33.9	180.0
NLDFT	30	58i	0.36	0.95	29.6	180.0
			10a			
HF	24	45i	−0.08	0.35	177.2	
MP2	30	40i	0.26	0.46	179.7	88.1
NLDFT	37	53i	0.11	0.60	175.6	84.9
			10b			
HF	24	38i	−0.06	1.76	33.4	5.3
MP2	37	26i	−0.09	1.79	35.1	7.5
NLDFT	40	38i	0.11	1.50	31.6	3.2
			11			
HF	24	15i	0.05	0.22	60.0	15.0
MP2	31	5i	0.20	0.39	60.0	15.0
NLDFT	28	62i	0.06	0.88	60.0	0.0

Wong and Wiberg have reported ground-state structures for **6** obtained at the HF level with basis sets up to 6-311++G** and also at the MP2/6-31G* and MP2/6-31+G** levels.[33] They obtain a H−C−Ca═O dihedral angle of 4.2° at the MP2/6-31G* level and 29.8° at the MP2/6-31G** level. Rotation barriers were not reported. We obtained an angle of 61.7° at the MP2/DZP level with a barrier of 0.21 kcal/mol. In order to provide more information about the surface, we repeated our calculations at the MP2 level with the aug-cc-pVDZ and aug-cc-pVTZ correlation-consistent basis sets.[34] At the MP2/aug-cc-pVDZ level, the torsion angle is 28.6° and the barrier is 0.02 kcal/mol. At the MP2/aug-cc-pVTZ level, the torsion angle is 56.0° and the barrier is 0.10 kcal/mol. The best calculations yield a torsion angle very similar to our MP2/DZP result with a barrier height that differs by only 0.11 kcal/mol. The MP2/aug-cc-pVTZ level barrier is in excellent agreement with the experimental value of 0.07 kcal/mol. All of these results demonstrate that the PES for CH_3 group rotation is very flat.

Experimental evidence regarding the preferred methyl rotamers of **6** is fully consistent with the MP2 results. Careful analysis of X-ray structure data allowed the assignment of methyl hydrogen positions in crystals of **6** and three ethanamide complexes.[14] The results yield H−C−C_a═O angles of 180(3)°, 175(4)°, 165(4)°, and 151(9)°, indicating that the inherently favored position of the methyl group is staggered with respect to the C_a═O. A neutron diffraction crystal structure of **6** at 23 K is also shown in Figure 2 for comparison.[17] In this structure the methyl group exhibits a H−C−C_a═O angle of 90°, halfway between being staggered (MP2) or eclipsed (HF) with the C_a═O bond. However, the thermal ellipsoids reveal a large degree of torsional freedom, which while consistent with a low barrier to rotation, make it difficult to confirm the geometry of the minimum energy conformation. Although early gas-phase electron diffraction data were insensitive to the rotation of the methyl group,[35] subsequent gas-phase studies showed that the best fit to electron diffraction data was obtained when the methyl group is staggered with respect to the C_a═O bond.[14]

The MM2 and MM3 force fields predict a minimum energy structure for **6** in which a methyl hydrogen eclipses the C_a═O bond.[9−12] The default MM3 force field yields a rotational barrier of 1.24 kcal/mol. The default MM3 force field was modified to obtain a better agreement with the MP2 PES. Marked improvement (see Figure 3) was obtained with the alteration of only one parameter, the V_3 term for the H−C−C_a−N torsion. With this minor modification MM3+ yields a minimum with an H−C−C_a═O dihedral angle of 180° and a rotational barrier of 0.21 kcal/mol.

Bond lengths and bond angles obtained at the various electronic structure levels and at the MM3+ level are compared with the gas-phase electron diffraction data and the neutron diffraction crystal structure for **6** in Table 2. Bond lengths obtained from electronic structure calculations (r_e) tend to be shorter than experimental values (r_g). The r_e values obtained

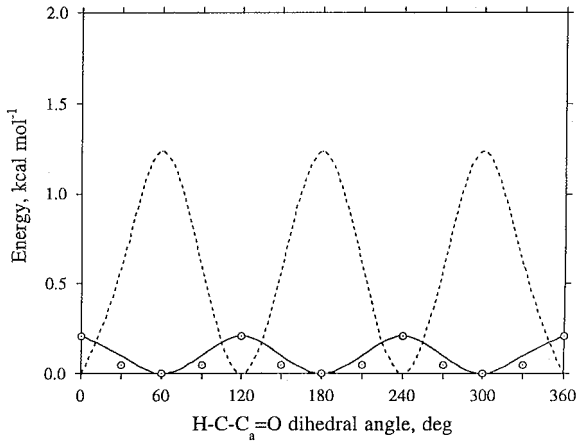

Figure 3. Comparison of MM3 PES for **6** with MP2 results: MP2 (⊙), default MM3 (− - −), MM3+ (−).

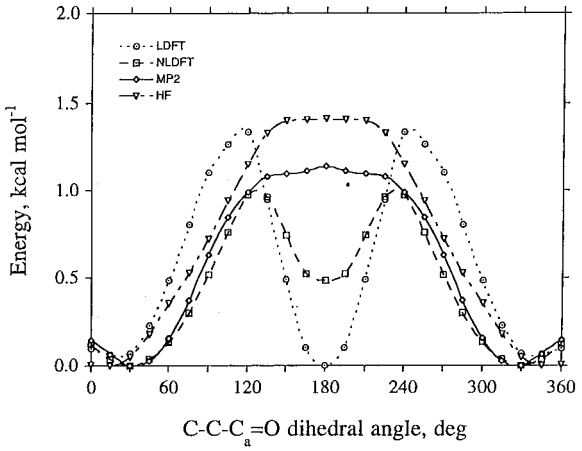

Figure 4. PES for **9** at various levels of theory.

from MP2 have been corrected to r_g values to allow a more meaningful comparison against the experimental and MM3+ results.[36] It can be seen that the agreement between the gas-phase electron diffraction data, MP2, and MM3+ ($\epsilon = 1.5$) results is quite good. Similarly, there is good agreement between the neutron diffraction crystal structure and MM3+ ($\epsilon = 4.0$). The HF geometry for **6** is similar to the MP2 geometry except for the C$_a$═O and C$_a$−N bond distances that are too short. The LDFT geometry is similar to the MP2 with the C$_a$−N bond distance 0.012 Å shorter than the MP2 value. The agreement between the NLDFT and MP2 structures is even closer with the largest differences found in the C−H and N−H bond distances.

Propanamide (9). The MP2 calculations yield a PES for the rotation of the ethyl group in **9** (Figure 4) with two symmetrical minima located at C−C−C$_a$═O dihedral angles of ∼±30° from 0°. These minima are broad with changes in energy of ≤0.15 kcal/mol in the range from −60° to 60°. A small barrier of only 0.15 kcal/mol separates the two minima. The fully optimized geometry for one of the minimum energy structures is shown in Figure 5 with the geometry parameters in Table 4. The MP2 calculation yields an optimal C−C−C$_a$═O dihedral angle of 33.9° in the absence of any torsional constraint on the ethyl group. Maxima occur at 0° as noted above and at 180° with a barrier height of 1.14 kcal/mol. The larger barrier at 180° is very broad and flat with little energy change in the region from 120° to 240°. Experimental barriers for this rotation are not available for comparison.

The HF PES is qualitatively similar to the MP2 PES with some specific differences. The barrier at 180° is still very broad

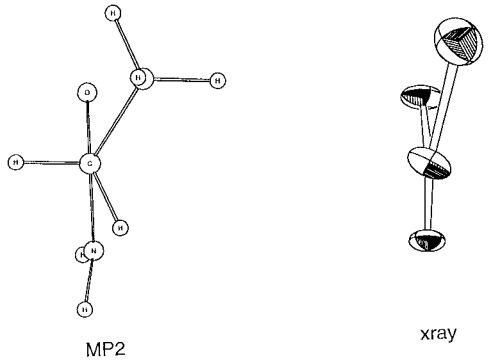

Figure 5. Comparison of the MP2 minimum energy structure and the X-ray crystal structure of **9** with thermal ellipsoids shown at 50% probability.[37]

and is 0.25 kcal/mol higher in energy than the MP2 barrier. The low barrier between the two minima has essentially disappeared at the HF level just as found for **6**. This shifts the minima at ∼± 30° toward 0°. The NLDFT PES for **9** (Figure 4) is similar to the MP2 PES in the region of the global minimum. The NLDFT surface has the global maximum at about 130° with a value of 1 kcal/mol. The NLDFT surface has a second minima at 180°, 0.5 kcal/mol above the global minimum. This is in contrast to the MP2 surface, which shows a broad, flat maximum in the region from 120° to 180°. The LDFT surface is grossly different from the MP2 surface. The global maximum is at ∼120° and is 1.35 kcal/mol above the global minimum. The global minimum is now at 180° with the 2 minima at ∼± 20°, 0.05 kcal/mol higher in energy. We note that even the larger of the rotation barriers are quite small, 0.33 to 0.5 that of the rotation barrier in C_2H_6, and that the MP2 and DFT energy differences are not large in an absolute sense. However, it is clear that the LDFT method, in particular, does not reproduce the MP2 PES. This is likely due to the well-established propensity at the LDFT level for overbinding which, in general, leads to too little repulsion in the van der Waals region.

The MP2 torsional frequency is 36 cm^{-1} (0.10 kcal/mol) (see Table 3). Thus the broad minimum can support a number of torsional vibrational levels. Furthermore, the zero-point energy correction to the barrier height is only 0.13 kcal/mol. This correction would lower the MP2 barrier to 1.0 kcal/mol. The HF torsional frequency (190 cm^{-1}, 0.54 kcal/mol) is much higher than the MP2 frequency and the HF potential would only support 2 to 3 torsional modes. The flatness of the HF PES near 180° leads to a near zero frequency (slightly positive) for the torsional motion. The zero-point energy correction of −0.36 leads to an increase of the barrier to 1.78 kcal/mol at the HF level. The NLDFT torsional frequency at the minimum is similar to the MP2 value whereas at the barrier the NLDFT imaginary frequency is twice the MP2 value consistent with the differences in the form of the PESs. The NLDFT barrier is reduced to 0.59 kcal/mol by the zero-point energy correction of 0.36 kcal/mol.

Crystal structure evidence regarding the preferred ethyl rotamers of **9** is fully consistent with the MP2 results which show that the C−C−C$_a$═O dihedral angle can adopt values ranging from −60° to +60° without gaining more than 0.15 kcal/mol. The X-ray crystal structure of **9** (see Figure 6) exhibits a C−C−C$_a$═O angle of 10°.[37] The Cambridge Structural Database[38] was searched to examine the rotational minima of other amides in which the carbonyl carbon was substituted with primary alkyl groups. A distribution of the C−C−C$_a$═O angles in 32 amides of the type X−CH$_2$−CH$_2$−C(═O)NH$_2$ (X = H

TABLE 4: Experimental and Calculated Structural Data for 9[a]

	r_e				r_g	MM3+	expt	MM3+
feature	LDFT	NLDFT	HF	MP2	MP2[b]	($\epsilon = 1.5$)	X-ray[c]	($\epsilon \geq 4.0$)
C_a═O	1.232	1.240	1.202	1.234	1.224	1.219	1.25	1.235
C_a−N	1.364	1.382	1.361	1.378	1.384	1.377	1.33	1.336
C_a−C	1.513	1.535	1.521	1.525	1.531	1.531	1.48	1.530
C−C	1.514	1.536	1.526	1.530	1.536	1.530	1.50	1.530
C−C_a═O	123.0	123.3	123.2	123.0		121.7	121	121.6
N−C_a═O	121.8	121.7	121.8	122.0		122.4	122	122.7
C−C_a−N	115.1	115.1	115.0	114.9		115.9	117	115.7
C_a−C−C	111.8	112.7	112.9	111.6		112.0	116	112.0

[a] Bond lengths in Å, bond angles in deg. [b] MP2 r_g values were estimated from computed r_e values based on past performance.[36] [c] X-ray diffraction crystal structure (Rfac = 0.084) of **9**.37

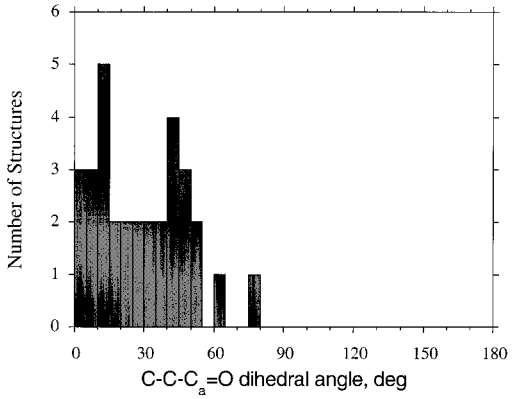

Figure 6. Distribution of C−C−C_a═O dihedral angles in 32 crystal structures containing the fragment X−CH_2−CH_2−C(═O)NH_2 where X = H or C(sp^3) (Cambridge Structural Database, January 1998 release).[38] Values range from 0.8°−77° with an average of 29.0°.

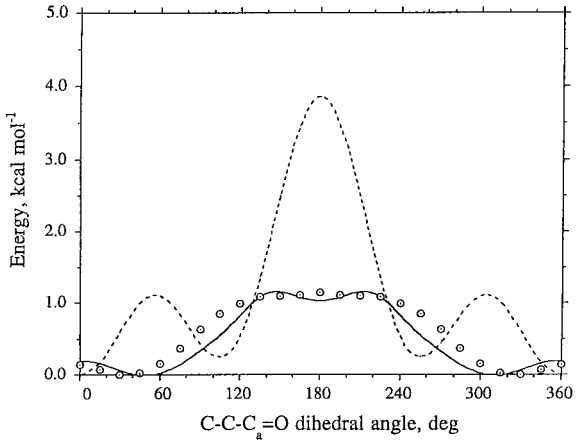

Figure 7. Comparison of MM3 PES for **9** with MP2 results: MP2 (⊙), default MM3 (− − −), MM3+ (—).

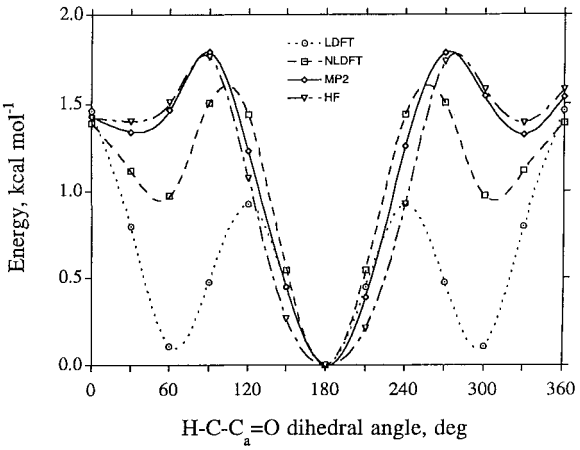

Figure 8. PES for **10** at various levels of theory.

or C(sp^3)) is shown in Figure 6. The values range from 1° to 77° with a mean value of 29°. This value is in remarkable agreement with the optimal value of 34° predicted for **9** at the MP2 level and can be compared to the torsion angles of 15°, 30°, and 15° predicted at the HF, NLDFT, and LDFT levels, respectively.

In contrast to the MP2 results which yield a single minimum on going from 0° to 180°, we observe that the default MM3 force field gives the global minimum at 0°, a maximum at 60°, 1.10 kcal/mol above the global minimum, a secondary minimum at 105°, and a maximum at 180°, 0.25 kcal/mol above the 105° minimum and 3.87 kcal/mol above the global minimum. The default MM3 force field was further modified to obtain a better fit with the MP2 PES. Marked improvement (Figure 7) was obtained by adjusting the V_1, V_2, and V_3 parameters for the C−C−C_a−N torsion interaction.

The modified torsional parameters, which were obtained by simultaneously fitting the rotational surface for **9** and **10** (vide infra), do not exactly reproduce the MP2 PES for **9** in that the two minima occur at ±45° rather than ±34°. In addition, MM3+ yields a small secondary minimum (depth of 0.1 kcal/mol), rather than a maximum, at 180°. We note, however, that the MM3+ parameters generally reproduce the behavior yielding the two broad minima separated by a 0.2 kcal/mol barrier at 0° and a 1.2 kcal/mol barrier for rotating past the NH_2 group at 180°.

Bond lengths and bond angles obtained with the various electronic structure levels and MM3+ are compared with the X-ray diffraction crystal structure for **9** in Table 4. As with **6**, there is good agreement between the MP2 and MM3+ (ϵ = 1.5) bond lengths and bond angles. Similarly, there is reasonable agreement between the X-ray diffraction crystal structure and MM3+ (ϵ = 4.0) bond lengths and angles. The *R* factor for this structure is high, suggesting that the experimental values may not be that reliable and the calculated values are more likely to best represent the gas-phase geometry parameters. The HF bond distances are shorter than the MP2 values, especially for the C═O bond length which is 0.032 Å shorter. The LDFT and NLDFT values are in reasonable agreement with the MP2 values. The LDFT distances tend to be shorter than the MP2 values by up to 0.02 Å. The NLDFT values are quite similar to the MP2 values, in general longer by ∼ 0.005 Å.

2-Methylpropanamide (10). The MP2 calculations yield a PES for the rotation of the isopropyl group in **10** (Figure 8) with a global minimum at an H−C−C_a═O dihedral angle of 180° and two symmetry-related minima at ∼±30°. Fully optimized geometries for the 180° minimum (**10a**) and one of the 30° forms (**10b**) are shown in Figures 9 and 10, respectively. In the absence of any torsional constraint on the H−C−C_a═O

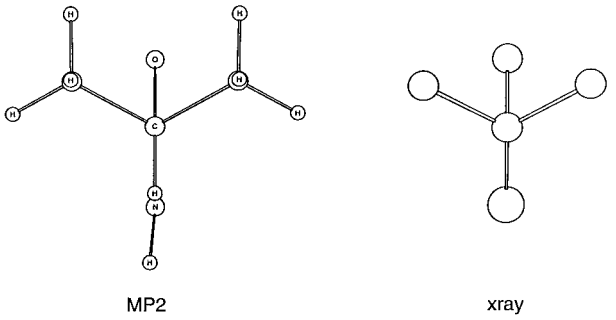

Figure 9. Comparison of the MP2 minimum energy structure and the X-ray crystal structure of **10a**.[39] Thermal ellipsoids are not rendered as anisotropic thermal parameters for this structure are unavailable.

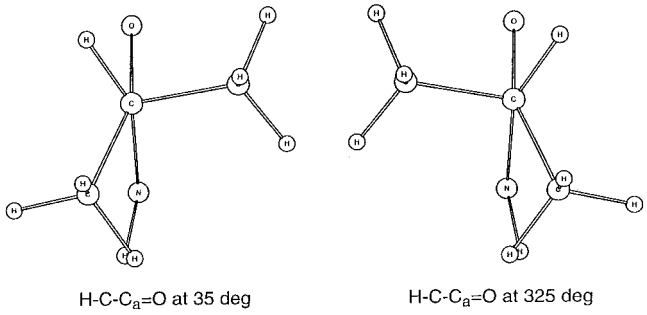

Figure 10. MP2 structures for **10b**.

dihedral angle, the minima are located at 180.0° and ± 35.0° with an energy difference of 1.34 kcal/mol. Maxima occur at ∼± 90° with a barrier height of 1.79 kcal/mol and at 0° with a barrier height of 1.43 kcal/mol above the global minimum. A barrier of only 0.09 kcal/mol thus separates the two high-energy minima. Experimental barriers for this rotation are not available for comparison.

The HF surface is very similar to the MP2 surface. The major difference is that the high-energy minimum is now 1.40 kcal/mol above the global minimum and the two high-energy minima are separated by a barrier of only 0.02 kcal/mol, reminiscent of the low HF barriers for **6** and **9**. Prior electronic structure calculations on **10** at the HF/4-31G* level also yield a global minimum when the hydrogen is anti to C$_a$=O.[20] However, in contrast to the MP2 or our HF results, the HF/4-31G* calculations yield a single maximum of 3.3 kcal/mol near an H−C−C=O angle of 60° and a second minimum in which the hydrogen is eclipsed with C$_a$=O (H−C−C$_a$=O dihedral angle of 0°). This is similar to our result in that a very low energy barrier separates the two minima. The energy difference between the minima at the HF/4-31G* level was 0.7 kcal/mol.

As expected from the calculations on **9**, the NLDFT PES (Figure 8) is similar to the MP2 PES for **10**. The location of the NLDFT secondary minima is similar to that of the MP2 minima but is found in a deeper well and is 0.97 kcal/mol above the global minimum. The two secondary minima are separated from the global minimum by a barrier of 1.50 kcal/mol and from each other by a barrier of 0.42 kcal/mol. The LDFT surface is again very different with the secondary minima only 0.11 kcal/mol above the global minimum. The secondary minima are separated from the global minimum by a barrier of 0.47 kcal/mol and from each other by a barrier of 1.37 kcal/mol. Thus the global barrier is at 0° as compared to the other PESs. It is useful to note that all of the methods give the energy difference between the 0° and 180° structures to be essentially the same.

The frequency analysis (see Table 3) is consistent with previous discussions. The MP2 torsion frequency at the global minimum is low, 30 cm^{-1} as expected. The MP2 zero-point energy correction is 0.26 kcal/mol for the energy difference between the global minimum and maximum lowering the barrier height to 1.53 kcal/mol. The torsion frequency at the secondary minimum is 37 cm^{-1} (0.10 kcal/mol), comparable to the barrier height of 0.09 kcal/mol. The small structural differences between the secondary minima and the secondary maximum lead to a zero-point correction that increases the barrier height by 0.09 kcal/mol at the MP2 level. These results suggest that the potential is very anharmonic in this region of the PES and that the secondary minimum may not support a vibrational level.

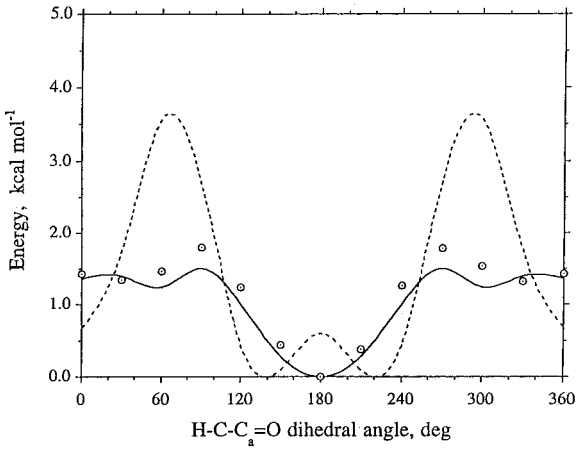

Figure 11. Comparison of MM3 PES for **10** with MP2 results: MP2 (⊙), default MM3 (− − −), MM3+ (−).

Experimental evidence regarding the preferred isopropyl rotamers of **10** is fully consistent with the MP2 results. The X-ray crystal structure of **10** (see Figure 9) exhibits C−C−C$_a$=O dihedral angles of 62.5° and −61.4° in accord with the calculated value of ±60.4° for the global minimum (H−C−C$_a$=O of 180.0°).[39] The same conformation is observed in crystal structures of other amides in which the carbonyl carbon is substituted with secondary alkyl groups, e.g., 2-butylhexaneamide[40] and 2-methyl-5-oxo-5-phenylpentanamide.[41] The other MP2 minima with H−C−C$_a$=O dihedral angles of ± 35.0° and C−C−C$_a$=O dihedral angles of ±80.0° and ±156.4° have not been experimentally observed. This is in accord with PES which shows that the barrier to move from the higher energy minima to the global minimum is small (0.47 kcal/mol) and that these minima are ∼1.3 kcal/mol above the global minimum and would not be populated thermally.

The PESs obtained with the default MM3 force field and the MM3+ force field are shown in Figure 11. The default MM3 parameters give a PES in which none of the minima correspond to the MP2 results. However, with the modifications to H−C−C$_a$−N and C−C−C$_a$−N torsional parameters (vide supra), MM3+ gives a PES that generally reproduces the features obtained with MP2. MM3+ yields a global minimum at an H−C−C$_a$=O dihedral angle of 180° and two symmetrical minima at ±60° with a relative energy of 1.23 kcal/mol. In addition, there is a small (depth of 0.05 kcal/mol) minimum at 0°. Maxima occur at ±95° with a barrier height of 1.51 kcal/mol and at ±25° with a barrier height of 1.41 kcal/mol.

Bond lengths and bond angles obtained by the electronic calculations and MM3+ are presented in Tables 5 and 6 for the different minima. As with **6** and **9**, there is good agreement between the MP2 and MM3+ ($\epsilon = 1.5$) bond lengths and bond angles. The HF geometry parameters show the same shortening as previously observed. The NLDFT and MP2 geometries are in reasonable agreement with each other with the NLDFT heavy

TABLE 5: Experimental and Calculated Structural Data for the 180° Form of 10[a]

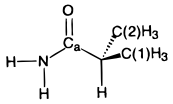

feature	re LDFT	re NLDFT	re HF	re MP2	r_g MP2[b]	MM3+ ($\epsilon = 1.5$)	expt X-ray[c]	MM3+ ($\epsilon \geq 4.0$)
C_a=O	1.233	1.240	1.204	1.235	1.225	1.219	1.230	1.235
C_a−N	1.363	1.383	1.359	1.375	1.381	1.377	1.320	1.336
C_a−C	1.517	1.541	1.524	1.525	1.531	1.536	1.503	1.536
C−C_1	1.526	1.549	1.533	1.534	1.540	1.538	1.500	1.538
C−C_2	1.514	1.538	1.533	1.534	1.540	1.538	1.492	1.538
C−C_a=O	122.9	123.3	122.1	122.4		121.6	121.2	121.5
N−C_a=O	122.0	121.5	121.8	122.2		122.3	121.4	122.6
C−C_a−N	115.1	115.2	116.1	115.5		116.0	117.4	115.9
C_a−C−C_1	110.1	110./6	109.4	109.0		110.4	111.2	110.4
C_a−C−C_2	107.7	108.7	109.4	109.0		110.4	111.3	110.4
C_1−C−C_2	111.0	111.4	111.6	111.0		110.2	110.7	110.0

[a] Bond lengths in Å, bond angles in deg. [b] MP2 r_g values were estimated from computed r_e values based on past performance.[36] [c] X-ray diffraction crystal structure (Rfac = 0.076) of **10**.[39]

TABLE 6: Experimental and Calculated Structural Data for the 35° Form of 10[a]

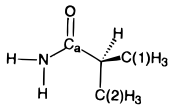

feature	r_e LDFT	r_e NLDFT	r_e HF	r_e MP2	r_g MP2[b]	MM3+ ($\epsilon = 1.5$)
C_a=O	1.235	1.242	1.204	1.236	1.226	1.220
C_a−N	1.361	1.379	1.360	1.377	1.383	1.378
C_a−C	1.519	1.540	1.525	1.527	1.533	1.541
C−C_1	1.522	1.548	1.537	1.538	1.544	1.539
C−C_2	1.517	1.541	1.532	1.532	1.538	1.527
C_a=O	121.5	121.6	121.1	121.7		120.0
N−C_a=O	121.8	121.5	121.4	121.7		121.2
C−C_a−N	116.7	116.8	117.5	116.5		118.9
C_a−C−C_1	108.4	109.1	108.7	108.3		110.0
C_a−C−C_2	115.3	115.1	115.1	115.0		115.0
C_1−C−C_2	111.5	111.8	111.6	111.4		109.7

[a] Bond lengths in Å, bond angles in deg. [b] MP2 r_g values were estimated from computed r_e values based on past performance.[36]

atom bond lengths being 0.004 Å longer than the MP2 values. The LDFT values are shorter than the MP2 values by a comparable amount. There is a fair agreement between the X-ray diffraction crystal structure and MM3+ ($\epsilon = 4.0$) bond lengths and angles. The discrepancies between calculated and experimental C−C bond distances suggest possible problems with this X-ray structure.

2,2-Dimethylpropanamide (11). The MP2 calculations yield a PES for the rotation of the tertiary butyl group in **11** (Figure 12) with global minima at C−C−C_a=O dihedral angles of ±60° and 180°. In addition, there are three shallow minima (0.02 kcal/mol) at 0° and ±120°. A fully optimized geometry for the 60° minimum is shown in Figure 13. The barrier to rotation is 0.39 kcal/mol. Experimental barriers for this rotation are not available for comparison. The X-ray crystal structure for this amide has not been reported.

The HF PES (Figure 12) follows the MP2 surface except that the barrier is essentially one-half of the MP2 value, 0.22 kcal/mol as compared to 0.39 kcal/mol. Again, the HF surface is going toward free rotation about the C_a−C bond. The NLDFT torsional PES is similar in form to the MP2 surface (Figure 12) except that the barrier of 0.9 kcal/mol is about twice as high as the MP2 value. As a consequence, the small secondary minima

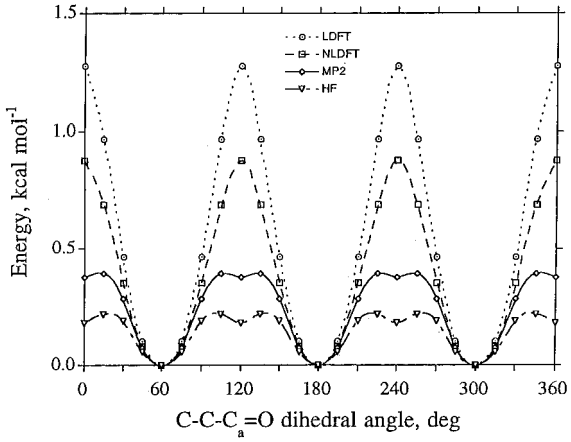

Figure 12. PES for **11** at various levels of theory.

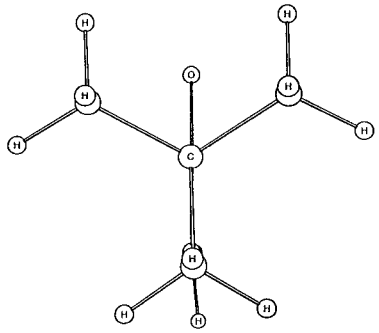

Figure 13. MP2 structure for the 60° form of **11**.

disappear at the NLDFT level. The LDFT PES (Figure 12) has an even higher barrier of 1.28 kcal/mol with the same form.

The surface in the region of the maximum at the MP2 level is very flat consistent with a near-zero imaginary frequency. The zero-point energy correction (see Table 3) to the torsional motion of 0.20 kcal/mol would lead to a barrier of only 0.19 kcal/mol if the frequencies can be treated as harmonic. These results are consistent with almost free rotation about the C_a−C bond in **11**.

The PESs obtained with the default MM3 force field and MM3+ are shown in Figure 13. In contrast to the MP2 results, the default MM3 parameters give a rotational potential surface in which there are three minima at 0° and ± 120° with a rotation barrier of 2.59 kcal/mol. However, with the modifications to

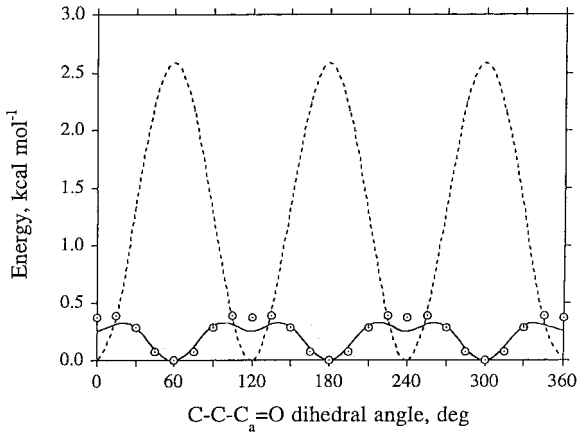

Figure 14. Comparison of MM3 PES for **11** with MP2 results: MP2 (⊙), default MM3 (− − −), MM3+ (—).

TABLE 7: Experimental and Calculated Structural Data for 11[a]

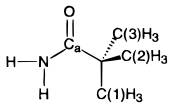

feature	r_e LDFT	NLDFT	HF	MP2	r_g MP2[b]	MM3+ ($\epsilon = 1.5$)
C_a═O	1.235	1.243	1.205	1.237	1.225	1.220
C_a−N	1.361	1.378	1.359	1.374	1.380	1.378
C_a−C	1.528	1.555	1.538	1.536	1.542	1.548
C−C_1	1.519	1.544	1.536	1.533	1.539	1.532
C−C_2	1.525	1.550	1.539	1.538	1.544	1.543
C−C_3	1.524	1.550	1.539	1.538	1.544	1.543
C−C_a═O	121.4	121.5	120.8	121.3		120.0
N−C_a═O	121.6	120.9	120.8	121.3		120.9
C−C_a−N	117.0	117.5	118.4	117.4		119.0
Ca−C−C_1	113.7	114.0	113.9	114.0		114.0
C_a−C−C_2	106.5	106.9	107.0	107.0		109.0
C_a−C−C_3	106.7	106.9	107.2	106.7		109.0
C_1−C−C_2	110.1	109.7	109.5	109.6		108.0
C_1−C−C_3	110.2	109.6	109.5	109.7		108.0
C_2−C−C_3	109.4	109.6	109.6	109.5		108.4

[a] Bond lengths in Å, bond angles in deg. [b] MP2 r_g values were estimated from computed r_e values based on past performance.[36]

H−C−C_a−N and C−C−C_a−N torsional parameters (vide supra), MM3+ gives a PES that reproduces the features obtained with MP2/dzp with global minima at ±60° and 180° and shallow minima at 0° and ±120°. The MM3+ barrier height is 0.31 kcal/mol. This result provides a validation that the modified MM3+ torsional parameters obtained by fitting to results for **9** and **10** are able to predict the rotational potential surface for **11**.

Bond lengths and bond angles obtained by MP2 and MM3+ are presented in Table 7. Again there is good agreement between the MP2 and MM3+ ($\epsilon = 1.5$) bond lengths and bond angles. The HF, NLDFT, and LDFT geometry parameters show the same behavior as previously observed for the other structures.

Conclusions

The potential energy surfaces for rotation about the C(sp^2)−C(sp^3) bond in calculated for acetamide (**6**), propanamide (**9**), 2-methylpropanamide (**10**), and 2,2-dimethylpropanamide (**11**) have been shown to be incorrectly predicted with the MM3 in comparison to MP2 calculations with a polarized double ζ basis set. A simple modification of two torsion interaction terms does lead to torsional potential energy surfaces in good agreement with the MP2 PESs. The maximum barriers to rotation (corrected for zero-point energy effects) are low, 0.22 kcal/mol for **6**, 1.01 kcal/mol for **9**, 1.53 kcal/mol for **10**, and 0.19 kcal/mol for **11**. The HF surfaces calculated with a good polarized double ζ basis set are in qualitative agreement with the MP2 surfaces and show a tendency toward predicting more free rotation when the MP2 barriers are low. DFT calculations at the local and nonlocal levels show differing degrees of agreement with the MP2 calculations with the nonlocal surfaces exhibiting the same qualitative behavior as the MP2 PESs. The LDFT PESs show the largest differences, in some cases giving different global minima and maxima. In all cases, fully optimized geometries of rotational minima at all levels are consistent with gas-phase electron diffraction data and crystal structure data.

Acknowledgment. This work was supported by the Environmental Management Science Program under direction of the U.S. Department of Energy's Office of Basic Energy Sciences (ER-14), Office of Energy Research, and the Office of Science and Technology (EM-52), Office of Environmental Management. The authors acknowledge Dr. Jeffrey C. Bryan and Dr. Michael N. Burnett of Oak Ridge National Laboratory for their assistance in preparing crystal structure figures. Pacific Northwest National Laboratory is a multiprogram national laboratory operated by Battelle Memorial Institute for the DOE under Contract DE-AC06-76RLO1830.

Supporting Information Available: Cartesian coordinates of optimized structures in angstroms. This material is available free of charge via the Internet at http://pubs.acs.org.

References and Notes

(1) Zabicky, J. *The Chemistry of Amides*; Wiley-Interscience: New York, 1970.

(2) Sigel, H.; Martin, R. B. *Chem. Rev.* **1982**, *82*, 385.

(3) Clement, O.; Rapko, B. M.; Hay, B. P. *Coord. Chem. Rev.* **1998**, *170*, 203.

(4) (a) Cuillerdier, C.; Musikas, C.; Hoel, P.; Nigond, L.; Vitart, X. *Sep. Sci. Technol.* **1991**, *26*, 1229. (b) Ruikar, P. B.; Nagar, M. S.; Pai, S. A.; Subramanian, M. S. *J. Radioanal. Nucl. Chem.* **1991**, *150*, 473. (c) Condamines, N.; Musikas, C. *Solv. Extr. Ion Exch.* **1992**, *10*, 69. (d) Prabhu, D. R.; Mahajan, G. R.; Nair, G. M.; Subramanian, M. S. *Radiochim. Acta* **1993**, *60*, 109. (e) Nair, G. M.; Prabhu, D. R.; Mahajan, G. H.; Shukla, J. P. *Solv. Extr. Ion Exch.* **1993**, *11*, 831. (f) Cuillerdier, C.; Musikas, C.; Nigond, L. *Sep. Sci. Technol.* **1993**, *28*, 155. (g) Tian, Q.; Hughes, M. A. *Hydrometallurgy* **1994**, *36*, 79. (h) Borong, B.; Chaohong, S.; Yizhi, B.; Gaodong, W.; Jun, Q.; Zhengbai, C. *J. Radioanal. Nucl. Chem.* **1994**, *178*, 99. (i) Nigond, L.; Musikas, C.; Cuillerdier, C. *Solv. Extr. Ion Exch.* **1994**, *12*, 297. (j) Nakamura, T.; Miyake, C. *Solv. Extr. Ion Exch.* **1995**, *13*, 253. (k) Nair, G. M.; Mahajan, G. R.; Prabhu, D. R. *J. Radioanal. Nucl. Chem.* **1995**, *191*, 323. (l) Nigond, L.; Coudamines, N.; Cordier, P. Y.; Livet, J.; Madic, C.; Cuillerdier, C.; Musikas, C. *Sep. Sci. Technol.* **1995**, *30*, 2075. (m) Ruikar, P. B.; Nagar, M. S.; Subramanian, M. S.; Gupta, K. K.; Varadarajan, N.; Singh, R. K. *J. Radioanal. Nucl. Chem., Lett.* **1995**, *201*, 125. (n) Wang, Y.-S.; Sun, G.-X.; Xie, D.-F.; Bao, B.-R.; Cao, W.-G. *J. Radioanal. Nucl. Chem., Lett.* **1996**, *214*, 67. (o) Wang, Y.-S.; Shen, C.-H.; Yang, Y.-H.; Zhu, J.-K.; Bao, B.-R. *J. Radioanal. Nucl. Chem., Lett.* **1996**, *213*, 199. (p) Shen, C.; Bao, B.; Zhu, J.; Wang, Y.; Cao, Z. *J. Radioanal. Nucl. Chem., Lett.* **1996**, *212*, 187. (q) Beer, P.; Drew, M. G. B.; Grieve, A.; Kan, M.; Leeson, P. B.; Nicholson, G.; Ogden, M. I.; Williams, G. *J. Chem. Soc., Chem. Commun.* **1996**, 1117. (r) Sasaki, Y.; Choppin, G. *J. Radioanal. Nucl. Chem.* **1996**, *207*, 383. (s) Chan, G. Y. S.; Drew, M. G. B.; Hudson, M. J.; Iveson, P. B.; Lijenzin, J.-O.; Skalberg, M.; Spjuth, L.; Madic, C. *J. Chem. Soc., Dalton Trans.* **1997**, 649.

(5) (a) Konings, M. S.; Dow, W. C.; Love, D. B.; Raymond, K. N.; Quay, S. C.; Rocklage, S. M. *Inorg. Chem.* **1990**, *29*, 1488. (b) Aime, S.; Anelli, P. L.; Botta, M.; Fedeli, F.; Grandi, M.; Paoli, P.; Uggeri, F. *Inorg. Chem.* **1992**, *31*, 2422. (c) Morrow, J. R.; Amin, S.; Lake, C. H.; Churchill, M. R. *Inorg. Chem.* **1993**, *32*, 4566. (d) Geze, C.; Mouro, C.; Hindre, F.; Le Plouzennec, M.; Moinet, C.; Rolland, R.; Alderighi, L.; Vacca, A.; Simonneaux, G. *Bull. Soc. Chim. Fr.* **1996**, *133*, 267.

(6) Hay, B. P.; Clement, O.; Sandrone, G.; Dixon, D. A. *Inorg. Chem.* **1998**, *37*, 5887.

(7) McCammon, J. A.; Harvey, S. C. *Dynamics of Proteins and Nucleic Acids*; Cambridge University Press: Cambridge, UK, 1987.

(8) Bohm, H.; Brode, S. *J. Am. Chem. Soc.* **1991**, *113*, 7129.

(9) Tanabe, K.; Osawa, E.; Tsuzuki, S.; Uchimaru, T. *Chem. Express* **1987**, *2*, 329.

(10) Schnur, D. M.; Yuh, Y. H.; Dalton, D. R. *J. Org. Chem.* **1989**, *54*, 3779.

(11) Lii, J.-H.; Gallion, S.; Bender, C.; Wikstrom, H.; Allinger, N. L.; Flurchick, K. M.; Teeter, M. M. *J. Comput. Chem.* **1989**, *10*, 503.

(12) Lii, J.-H.; Allinger, N. L. *J. Comput. Chem.* **1991**, *12*, 186.

(13) Maple, J. R.; Hwang, M.-J.; Jalkanen, K. J.; Stockfish, T. P.; Hagler, A. T. *J. Comput. Chem.* **1997**, *19*, 430.

(14) Hagler, A. T.; Leiserowitz, L.; Tuval, M. *J. Am. Chem. Soc.* **1976**, *98*, 8, 4600.

(15) Fillaux, F.; Thomkinson, J. *Chem. Phys.* **1977**, *26*, 295.

(16) Kojima, T.; Yano, E.; Nakagawa, K.; Tsunekawa, S. *J. Mol. Spectrosc.* **1985**, *1985*, 494.

(17) Jeffrey, G. A.; Ruble, J. R.; McMullan, R. K.; DeFrees, D. J.; Binkley, J. S.; Pople, J. A. *Acta Crystallogr., Sect. B* **1980**, *36*, 2292.

(18) Radom, L.; Lathan, W. A.; Herhe, W. J.; Pople, J. A. *Aust. J. Chem.* **1972**, *25*, 1601.

(19) Sugawara, Y.; Hirakawa, A. Y.; Tsuboi, M.; Kato, S.; Morokuma, K. *J. Mol. Spectrosc.* **1986**, *115*, 21.

(20) Tasaki, K.; Suter, U. W. *J. Phys. Chem.* **1988**, *92*, 5886.

(21) *Gaussian 94*; Frisch, M. J.; Trucks, G. W.; Schlegel, H. B.; Gill, P. M. W.; Johnson, B. G.; Robb, M. A.; Cheeseman, J. R.; Keith, T. A.; Petersson, G. A.; Montgomery, J. A.; Raghavachari, K.; Al-Laham, M. A.; Zakrzewski, V. G.; Ortiz, J. V.; Foresman, J. B.; Cioslowski, J.; Stefanov, B. B.; Nanayakkara, A.; Challacombe, M.; Peng, C. Y.; Ayala, P. Y.; Chen, W.; Wong, M. W.; Andres, J. L.; Replogle, E. S.; Gomperts, R.; Martin, R. L., Fox, D. J.; Binkley, J. S.; Defrees, D. J.; Baker, J.; Stewart, J. J. P.; Head-Gordon, M.; Gonzalez, C.; Pople, J. A. Gaussian, Inc.: Pittsburgh, PA, 1995.

(22) (a) Andzelm, J.; Wimmer, E.; Salahub, D. R. In *The Challenge of d and f Electrons: Theory and Computation*; Salahub, D. R., Zerner, M. C., Eds.; ACS Symposium Series, No. 394; American Chemical Society: Washington, DC, 1989; p 228. (b) Andzelm, J. In *Density Functional Theory in Chemistry*; Labanowski, J., Andzelm, J., Eds.; Springer-Verlag: New York, 1991; p 155. (c) Andzelm, J. W.; Wimmer, E. *J. Chem. Phys.* **1992**, *96*, 1280. DGauss is a density functional program which is part of Unichem and is available from Oxford Molecular.

(23) Moller, C.; Plesset, M. S. *Phys. Rev.* **1934**, *46*, 618.

(24) Pople, J. A.; Binkley, J. S.; Seeger, R. *Int. J. Quantum Chem. Symp.* **1976**, *10*, 1.

(25) Dunning, T. H., Jr.; Hay, P. J. *Methods of Electronic Structure Theory*; Plenum Press: New York, 1977.

(26) (a) Parr, R. G.; Yang, W. *Density Functional Theory of Atoms and Molecules*. Oxford University Press: New York, 1989; (b) Labanowski, J.; Andzelm, J., Eds. *Density Functional Methods in Chemistry*. Springer-Verlag: New York, 1991. (c)Ziegler, T. *Chem. Rev.* **1991**, *91*, 651. (d) Salahub, D. R. In *Ab Initio Methods in Quantum Chemistry—II*; Lawley, K. P., Ed.; J. Wiley & Sons: New York, **1987**; p 447. (e) Jones, R. O.; Gunnarsson, O. *Rev. Mod. Phys.* **1989**, *61*, 689.

(27) Vosko, S. J.; Wilk, L.; Nusair, W. *Can. J. Phys.* **1980**, *58*, 1200.

(28) (a) Becke, A. D. *Phys. Rev. A* **1988**, *38*, 3098. (b) Becke, A. D. In *The Challenge of d and f Electrons: Theory and Computation*; Salahub, D. R., Zerner, M. C., Eds.; ACS Symposium Series, No. 394; American Chemical Society: Washington, DC, 1989; p 166. (c) Becke, A. D. *Int. J. Quantum Chem. Symp.* **1989**, *23*, 599.

(29) Perdew, J. P. *Phys. Rev. B* **1986**, *33*, 8822.

(30) Godbout, N.; Salahub, D. R.; Andzelm, J.; Wimmer, E. *Can. J. Chem.* **1992**, *70*, 560.

(31) *MM3(96)*. The program may be obtained from Tripos Associates, 1699 S. Hanley Road, St. Louis, MO 63144, for commercial users, and it may be obtained from the Quantum Chemistry Program Exchange, Mr. Richard Counts, QCPE, Indiana University, Bloomington, IN 47405, for noncommercial users.

(32) Allinger, N. L.; Chen, K.; Rahman, M.; Pathiaseril, A. *J. Am. Chem. Soc.* **1991**, *113*, 4505.

(33) Wong, M. W.; Wiberg, K. B. *J. Phys. Chem.* **1992**, *96*, 668.

(34) (a) Dunning, T. H., Jr. *J. Chem. Phys.* **1989**, *90*, 1007. (b) Kendall, R. A.; Dunning, T. H., Jr.; Harrison, R. J. *J. Chem. Phys.* **1992**, *96*, 6796. (c) Woon, D. E.; Dunning T. H., Jr. *J. Chem. Phys.* **1993**, *99*, 1914. (d) Peterson, K. A.; Kendall, R. A.; Dunning T. H., Jr. *J. Chem. Phys.* **1993**, *99*, 1930. (e) Peterson, K. A.; Kendall, R. A.; Dunning, T. H. Jr. *J. Chem. Phys.* **1993**, *99*, 9790. (f) Woon, D. E.; Dunning T. H., Jr. *J. Chem. Phys.* **1995**, *103*, 4572.

(35) Kitano, M.; Kuchitsu, K. *Bull. Chem. Soc. Jpn* **1973**, *46*, 3081.

(36) Ma, B.; Lii, J.-H.; Schaefer, H. F.; Allinger, N. L. *J. Phys. Chem.* **1996**, *100*, 8763.

(37) Usanmaz, A.; Adler, G. *Acta Crystallogr., Sect. B* **1982**, *38*, 660.

(38) Allen, F. H.; Bellard, S. A.; Brice, B. A.; Cartwright, A.; Doubleday: A.; Higgs, H.; Hummelink, T.; Hummelink-Peters, B. G.; Kennard, O.; Motherwell, W. D. S.; Rodgers, J. R.; Watson, D. G. *Acta Crystallogr., Section B* **1979**, *35*, 2331.

(39) Cohen-Addad, C.; Cohen-Addad, J.-P. *J. Chem. Soc., Perkin Trans. 2* **1978**, 168.

(40) Cohen-Addad, C.; Grand, A. *Acta Crystallogr., Sect. B* **1974**, *30*, 1342.

(41) Andreetti, G. D.; Bocelli, G.; Cybulski, J.; Dabrowski, Z.; Wrobel, J. T. *J. Mol. Struct.* **1985**, *128*, 259.